Bulletin of Earthquake Engineering
https://doi.org/10.1007/s10518-020-00785-4

ORIGINAL RESEARCH

Experimental and analytical studies of sub-standard RC frames retrofitted with buckling-restrained braces and steel frames

Fatih Sutcu[1] · Ahmet Bal[2] · Kazuhiro Fujishita[3] · Ryota Matsui[4] · Oguz C. Celik[5] · Toru Takeuchi[4]

Received: 8 August 2019 / Accepted: 3 January 2020

Abstract
Existing reinforced concrete (RC) buildings designed according to outdated codes may lack sufficient strength, stiffness or ductility to meet the seismic performance criteria of current codes. To enhance the system stiffness and re-centering capability, an elastically designed supplementary steel frame (SF) is installed in parallel with the BRBs. Near full-scale cyclic tests are conducted on such retrofit schemes for performance evaluation. The retrofitted specimens showed stable hysteretic behavior up to the retrofit target story drift of 1/150 as proposed in the Japanese seismic regulations. Tests demonstrate that the proposed system is feasible and increases both strength, ductility, and damping to an adequate seismic performance level while the elastic steel frame is effective in providing post-yield stiffness and re-centering capability even when the RC frame is subjected to moderate inelasticity. Special emphasis is placed on the composite behavior of RC members and SF. A simplified composite interaction model is proposed and results from the developed model show good agreement with the experimental data. Ductility demands are shown to concentrate in the BRBs as per the design intent.

Keywords Seismic retrofitting · Buckling-restrained braces · Elastic steel frame · Energy dissipation · Cyclic loading tests

✉ Fatih Sutcu
fatih.sutcu@itu.edu.tr

[1] Faculty of Civil Engineering, Istanbul Technical University, Istanbul, Turkey

[2] Graduate School of Science, Engineering and Technology, Istanbul Technical University, Istanbul, Turkey

[3] Kozo Keikaku Engineering, Tokyo, Japan

[4] Department of Architecture and Building Engineering, Tokyo Institute of Technology, Tokyo, Japan

[5] Structural and Earthquake Engineering Division, Faculty of Architecture, Istanbul Technical University, Istanbul, Turkey

Published online: 21 January 2020

1 Introduction

Existing RC buildings are typically deficient in multiple aspects, such as having insufficient lateral strength, stiffness, ductility or energy dissipation capacity. Older public buildings such as schools and hospitals pose a particular hazard, and often must be retrofitted to ensure safety during and after a major seismic event. Although conventional retrofitting methods such as addition of RC shear walls or classical (i.e. buckling) steel braces are widely used since experiences gained over the course of time are significant (JBDPA 2001).

Among the numerous retrofit solutions, steel braces have several notable advantages over RC shear walls. Steel members and subassemblies may be prefabricated, transported to construction site, and rapidly installed. Such systems are preferred by architects especially for improved daylighting. Additionally, steel braces are relatively light, and the strength and ductility can be tuned to meet project specific requirements.

In many retrofit applications, steel braces are attached directly to the RC frame or via an intermediary steel frame, which is connected to the existing RC frame with post-installed anchors. However, to better transmit the brace forces and improve the elastic stiffness, it is proposed to complement the steel braces with a closed steel moment frame. This system provides a larger increase in lateral capacity compared to encasing the columns with an RC jacket or adding new shear walls. Moreover, elastic range of the steel frame is generally larger compared to a retrofitted RC frame, enhancing the self-centering capability of the overall system. If the connection details and anchors between the RC and steel frames are properly designed and implemented, the retrofitted system's ultimate capacity is governed by yielding or buckling of the brace, column shear mechanism, or weld failure (Sugano 1989).

In conventional braces, while flexural buckling can be employed as the designated fuse mechanism, the compressive strength and stiffness are severely deteriorated upon buckling, resulting in a highly unsymmetrical hysteresis and requiring balanced tension–compression brace pairs. Furthermore, the unsightly damage of a buckled brace increases the post-earthquake repair cost. However, despite these challenges, properly designed and constructed braces of certain types (for example tubular braces having compact sections) can dissipate significant amounts of hysteretic energy (Celik et al. 2005).

Recently, buckling restrained braces (BRBs) have been gaining increasing use, both in lieu of conventional braces and to achieve higher performance targets. BRBs were first developed in Japan in early 1980's and used in an actual building in 1990 (Fujimoto et al. 1990). These braces are designed such that buckling is restrained, producing nearly symmetric hysteresis without visible damage, and attaining a significant proportion of the base core material's coupon test low cycle fatigue capacity. Applied as a retrofit, the combined frame hysteresis is also stable and reliable. The typical composition consists of a steel core with the area selected according to the required strength, and plastic length according to the desired yield drift. This core is encased in an axially decoupled steel restraining tube, which is filled with mortar, and provides the lateral stiffness to control the core buckling amplitude.

Stable and ductile characteristics enable this axially yielding device to function as a hysteretic damper to retrofit deficient frames. Basic principles and yielding mechanism of BRBs have been well documented (Wakabayashi et al. 1973; Watanabe et al. 1988), and recent studies have investigated the detailed component behavior, both analytically and experimentally (Palazzo et al. 2009; Wu et al. 2013). The interaction of BRBs in

sub-assemblages has also been studied extensively (Takeuchi et al. 2014, 2016; Chou and Liu 2012).

Analytical simulation and performance assessment of BRB-strengthened RC buildings and bridges have been conducted (Sabellia et al. 2003; Kiggins and Uang 2006; Celik and Bruneau 2009; El-Bahey and Bruneau 2011; Qu et al. 2012; Freddi et al. 2012; Barbagallo et al. 2019). Experimental studies have provided details where the BRB is connected to the RC frame using direct connections such as pre-loaded ties or post-fixed anchors (Dinu et al.2012; Yooprasertchai and Warnitchai 2008; Mahrenholtz et al. 2015). Other experimental studies have investigated the BRB retrofitting or strengthening of frames through pseudo dynamic tests. Ozcelik and Erdil (2019) tested RC frames strengthened by BRBs in a chevron configuration and confirmed the results with time-history analyses. Tsai et al. (2008) conducted a series of tests on BRB frames having concrete-filled tube (CFT) columns. In a cyclic field test, Della Corte et al. (2015) implemented all-steel dismountable BRBs applied in an existing damaged RC building. Note that direct connection of BRBs may result in concentrated damage to already weak RC beam-column joints. One of the first practical RC frame retrofit applications was reported in 2006 (Takeuchi et al. 2006). Although limited, more recent studies have investigated the seismic upgrading of RC frames with BRBs with various installation options (Pan et al. 2016; Di Sarno and Manfredi 2012). These research studies and real-life implementations reveal that there is potential for expanded use of BRBs as a convenient retrofit solution for low-ductility/low-strength RC structures.

To investigate the effectiveness of the proposed BRB retrofit scheme and provide an experimental validation, this paper presents a series of large-scale cyclic tests of RC frames retrofitted with BRBs. The tests indicate that the proposed scheme is feasible and increases strength as well as ductility to an adequate seismic performance level. The proposed BRB retrofit system includes a supplementary steel frame (SF) that is designed to remain elastic installed in parallel with the BRB in which SF enhances the system stiffness and restoring capability. All BRBs employed a low yield point steel core (LYP225) and were either welded or bolted to gusset plates integral to the SF. Connection between the RC and steel frames consists of steel studs, chemical anchors, ladder stirrups, and high-strength grout. This interface, denoted as the mortar zone, provides significant composite action, which is clearly identified in the test results. Special emphasis is placed on this composite behavior and a simplified semi-composite interaction model is proposed. Results from this analytical model have good agreement with the test results, while the simple non-composite model underestimates and fully composite behavior overestimates the interaction. Ductility demands are shown to concentrate in the BRBs, while the elastic steel frame is effective in providing post-yield stiffness and re-centering capability even when the RC frame is subjected to moderate inelasticity following an earthquake. The proposed retrofit application is expected to reduce the residual drifts, enhance self-centering features, and allows repairability of the building after a major seismic event. Moreover, the SF increases the axial, shear, and bending capacities of the involved RC columns, which is especially important in similar applications where the addition of the BRB members would increase the seismic demands on the columns. The obtained stable hysteresis and energy dissipation of the combined system demonstrate that employing BRBs with a supplementary steel frame is a promising technique to control the response of low-ductility and/or low-strength RC buildings posing a severe seismic hazard.

2 Outline of experiments

For the experimental part of this work, test frames representing a single bay from the ground story of a typical five-story RC Turkish school building are studied at near full scale. A typical five-story RC school building in Turkey is generally composed of RC moment resisting frames and shear walls. Again, typically, 3 and closely spaced 10–12 bays exist in such buildings in short and long plan directions, respectively. Retrofit work is generally required in the long direction where the number of shear walls is less (or when no shear walls are present) and the columns are working about the weak axis. Therefore, a longitudinal bay made with weaker frames is considered in this work. For such existing school buildings, the first elastic fundamental period is approximately in the range of 0.7–0.8 s. As for the seismic detailing, usually confinement regions are provided in the beam-to-column joint regions especially for school buildings that have been designed and constructed after the 1968 seismic code of Turkey. However, in practice, there are buildings that still do not meet the ductility requirements mandated by the codes. In such buildings, in addition to a selected system retrofit scheme, confinement measures should also be taken by implementing external intervention in the RC members such as FRP wrapping or steel jacketing. For the tested frames here, seismic detailing is already present in the frame members and therefore no additional confinement is needed. In these buildings, it is common for the beam and column inner faces to be aligned for architectural purposes. The proposed scheme features a BRB installed within a closed steel frame, which is designed to remain elastic and is placed within the existing RC frame (Fig. 1). Mortar infill confined with two layers of ladder shaped stirrups provide a shear connection between the existing RC frame via post-fixed anchors with epoxy bonding and shear studs welded to the steel section's web. Connection design selected here followed the Japanese retrofit design guidelines (JBDPA 2001).

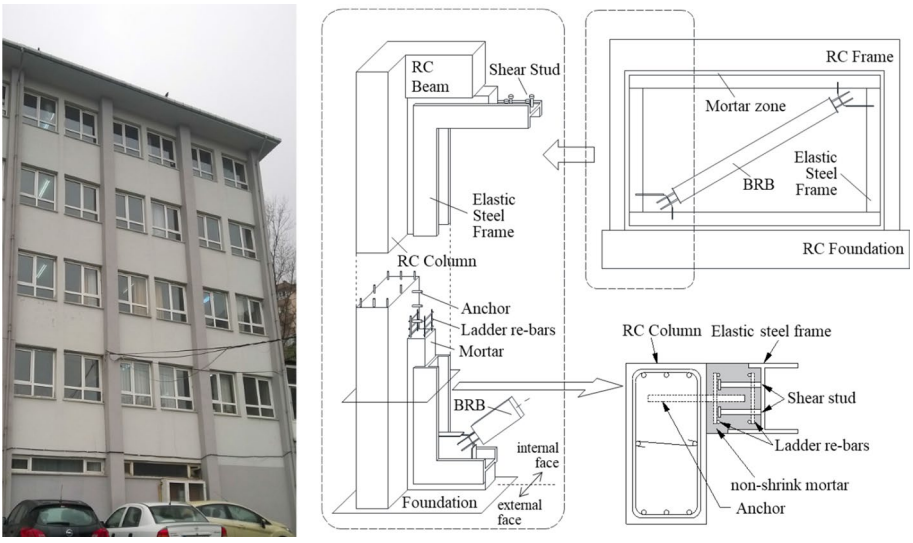

Fig. 1 Typical school building in Turkey (left) retrofit concept and RC to steel frame connection layout (right)

In previous experiments (Fujishita et al. 2015), the BRB component behavior was investigated comprehensively both for welded and bolted end connections where the BRB specimens were tested up to 3% axial strain level. The experimental program of this paper included four single bay specimens to confirm the existing RC frame and the retrofitted frame behavior, both at a connection and system levels. The test specimens are identified as:

- R model: Bare RC frame
- RS model: RC frame with concentric steel frame
- RSB model: RC frame with concentric steel frame and BRB
- RSBe model:RC frame with external/eccentric steel frame and BRB

RS model is investigated as an intermediate step of the proposed retrofit method where the test results could enable to distinguish the effect of steel frame. RSB and RSBe are retrofit options for different building conditions, although in the paper, the composite behavior is extensively explained on the RSB model for simplicity. In the RSB specimen, the steel frame and BRB are placed in-line with the RC beam in a concentric configuration while in the RSBe specimen they are placed externally to the beam in an eccentric configuration. In the RSBe configuration, there may be certain advantages such as minimum interruption to the building functions, as the new steel frame is located externally and the new steel columns can be continuous along the height of the building. Detailed dimensions of the structural components and connections are depicted in Figs. 2, 3 and 4.

The RC frame was designed based on conventional practice from the 1990's for school buildings, but scaled to 80% to accommodate the test facility size and load capacity limits. Reflecting the materials commonly employed at the time, C20 concrete ($f_{ck} \approx 20$ MPa) and

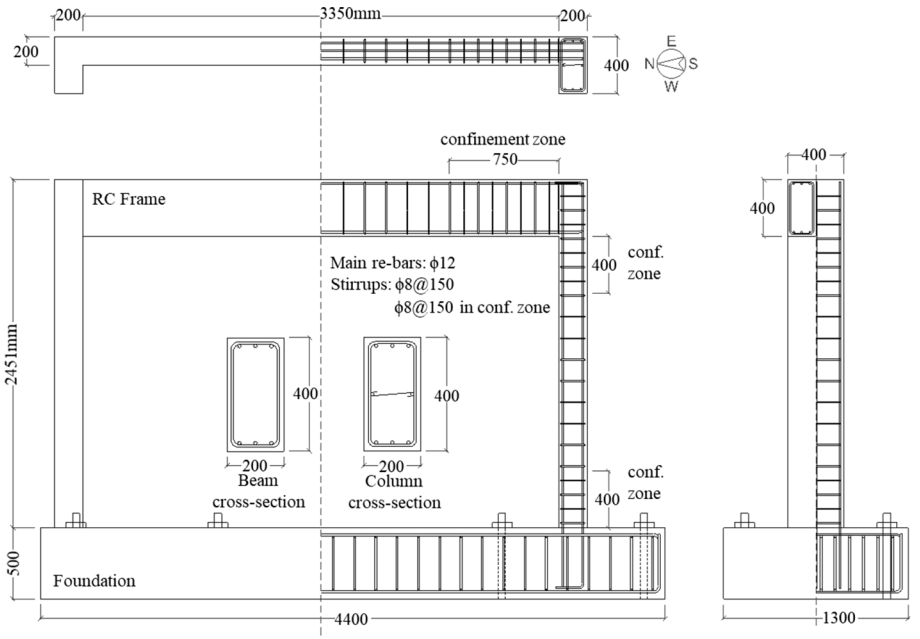

Fig. 2 Bare RC frame: R model

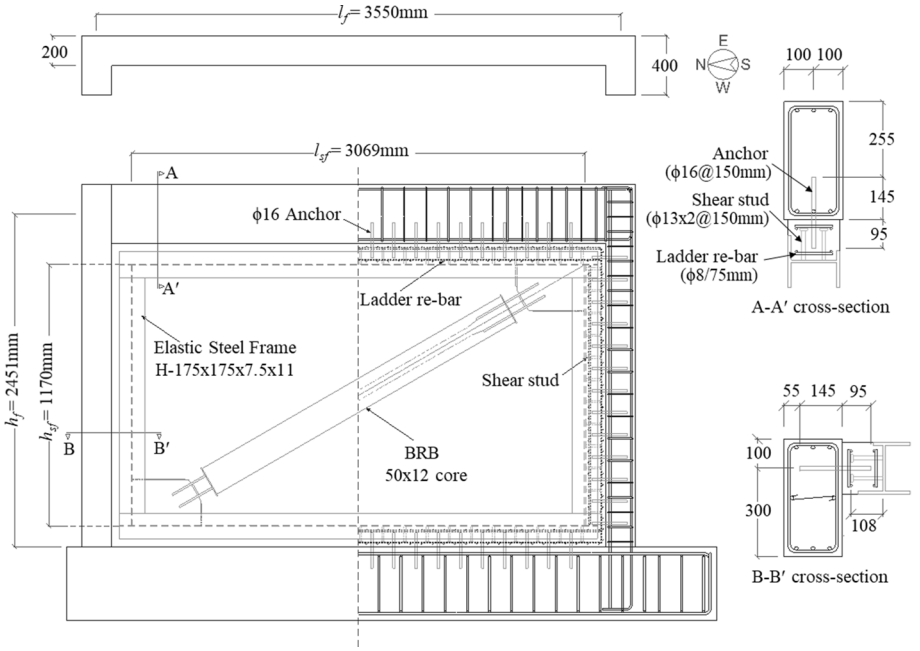

Fig. 3 RS and RSB model

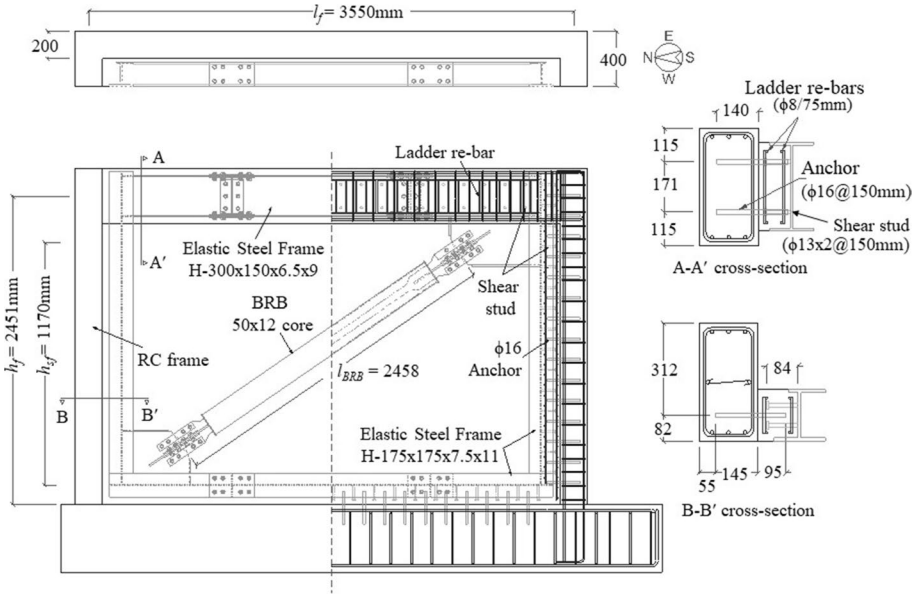

Fig. 4 RSBe model (external steel frame and BRB)

S420 rebar ($f_{yk} \approx 420$ MPa) were used. High strength mortar with a characteristic strength of 80 MPa was used to connect the steel and RC frames. Design of the RC frame, re-bar ratios and placement in RC frame followed the 1975 Turkish Seismic Code that was effective in 1990's (SSBDA 1975; TS-500 1975, 1984).

Design of the BRB follows an equivalent linearization method where the spectral response is modified according to the stiffness and equivalent damping. The BRB design is considered in terms of the ratio of BRB stiffness to the initial stiffness of RC frame (K^{BRB}/K_0^{RC}) although the final design depends on the stiffness of each component at the target displacement, which is extensively explained in previous publications (Sutcu et al. 2014; Takeuchi and Wada 2017). The behaviors of each component and the total system are estimated using the assumed initial behavioral values such as stiffness. As for reference, in this study, the K^{BRB}/K_0^{RC} ratios for RSB and RSBe specimens are 2.6 and 2.8, respectively. The BRBs used in the experiments are composed of a 50 mm × 12 mm, LYP225 grade steel core and 175 × 175 × 4mm STKR400 grade steel square restrainer tube. As for the BRB connections, two different connection types were used to better understand the applicability of the proposed two methods. A welded type connection was used in RSB specimen whereas bolted type was implemented in the RSBe specimen. Both connections constitute a similar end rotational stiffness for comparability. Welded type connection provides more flexible erecting and site adjustment possibility while bolted type requires a more precise application technique.

The steel frame is designed to remain elastic within the target displacement range approximately up to 1% story drift ratio. As there are chemical anchors on the RC frame, half of the flange is cut in steel members for easily sliding the steel frame into place (Figs. 3 and 4 cross-sections). The ratio of steel frame stiffness to the BRB stiffness (K^{SF}/K^{BRB}) for such retrofit applications is generally between 4 and 10%. In this study, K^{SF}/K^{BRB} ratio is designed to be approximately 10%. Average coupon test strengths for the BRB core, restrainer tube, and the steel frame are given in Table 1.

A displacement based loading protocol is developed for this test program and is shown in Fig. 5. In the initial stages, the BRB is expected to yield, and the story drift is set to be 1/3, 2/3 or 3/3 of the estimated RC frame yield drift 1/225 (0.44%). This is followed by cycles at the retrofit target drift of 1/150 (0.67%) which is designated according to the Japanese seismic guideline (JBDPA 2001) and Turkish Seismic Code (TBSC-2018) and cycles at 1/100 drift (1.0%), which is the life safety (LS) performance level drift limit prescribed in several international seismic codes. Finally, higher amplitude cycles at 2.0% and 3.0% story drifts are applied to observe the behavior under large displacements. However, not all specimens were subjected to the whole loading protocol, as the testing device reached its maximum capacity at around 1% drift for the stronger retrofitted specimens.

To represent the weight of the upper stories, a constant axial load of 250 kN was initially applied to each column, corresponding to 15% of the column's axial capacity. The actuator

Table 1 Material characteristic of steel frame, BRB core, and restrainer tube

Steel member	Type of material	Yield stress (MPa)	Ultimate stress (MPa)
BRB core plate	LYP225	235	305
Restrainer tube	STKR400	381	467
Steel frame H-175 × 175 × 7.5 × 11	SM490	402	529

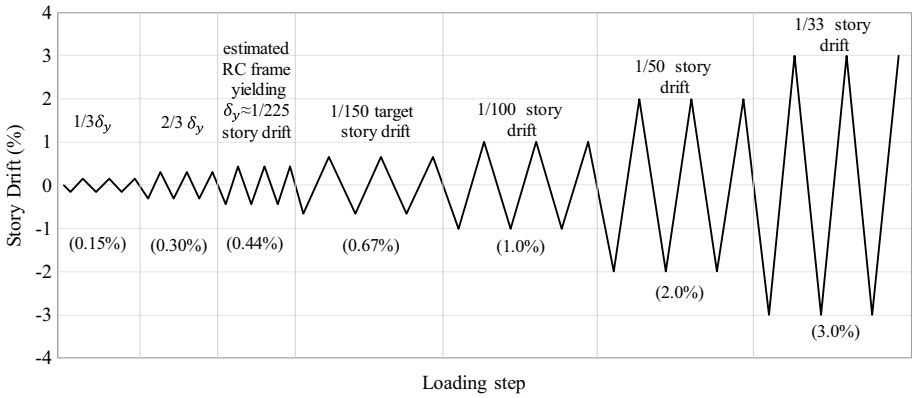

Fig. 5 Loading protocol

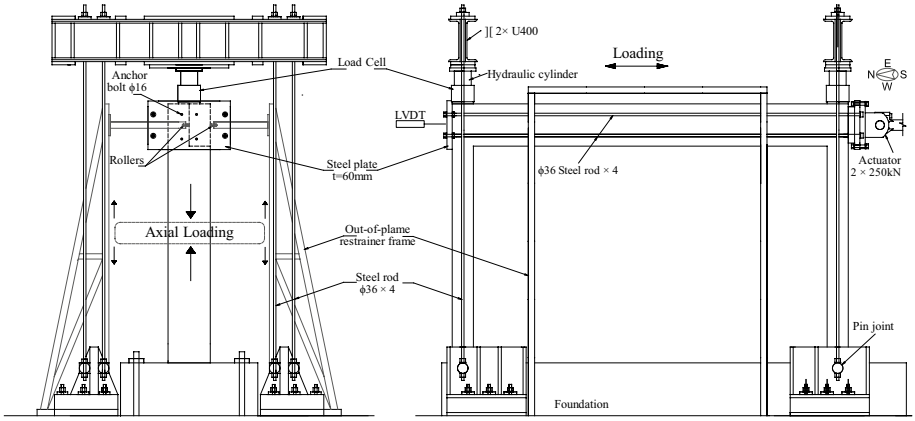

Fig. 6 Horizontal cyclic loading and axial load system

and axial loading system details are shown in Fig. 6 and all test specimens in the test set-up are given in Fig. 7.

The specimens were instrumented with strain gauges attached to the RC main rebars and stirrups, the BRB restrainer and neck (i.e. core extension), the steel frame, and selected post-fixed anchors and studs. Both in-plane and out-of-plane frame BRB deformations, as well as RC frame and steel frame deformations were measured using LVDTs. The axial deformation of the BRB was also measured using wire-type LVDTs attached to the restrainer end and neck, while differential deformation between the RC and steel frames was measured using pi-type strain gauges.

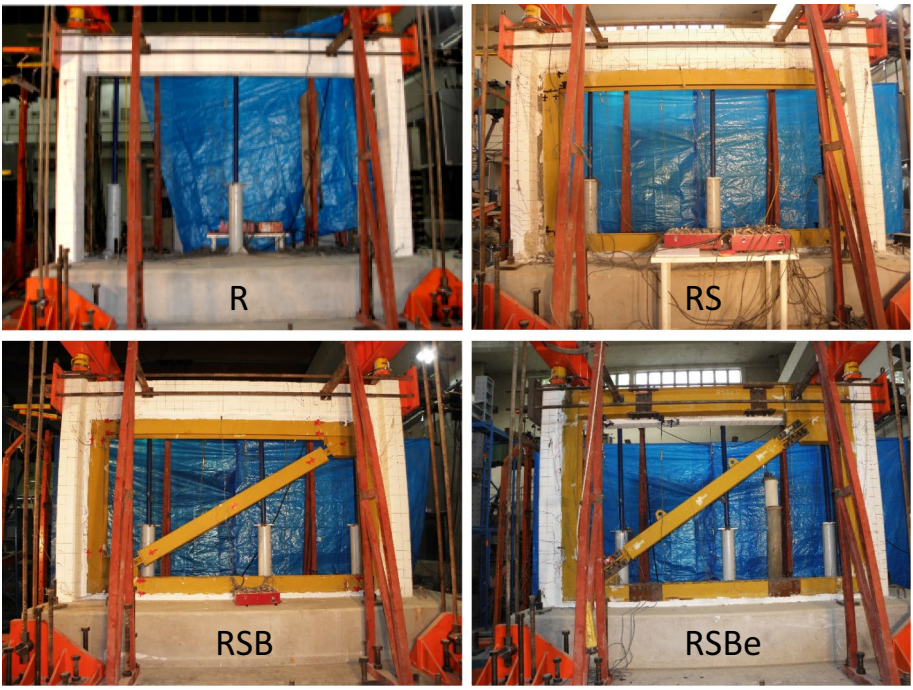

Fig. 7 Test specimens and test set-up

3 Experimental behavior of specimens

Although first two specimens are loaded up to higher drift levels, for easier comparison, cyclic test results for the specimens up to 1% drift are shown in Fig. 8 in terms of horizontal load versus displacement (and story drift angle) hysteresis. Experimental response of the R specimen (bare RC frame) is shown in Fig. 8a, with the RC frame exhibiting stable inelastic behavior. Note that observed cracks were small in width and length. According to the test results, the initial stiffness was calculated to be $K_0^{RC} = 17.33$ kN/mm. No significant cracks were observed at the retrofit target story drift angle of 1/150 (maximum crack width: 0.75 mm). Following 9 full cycles at 3% story drift, additional cycles at 4% story drift were conducted before terminating the test. A flexural failure was observed with exposed rebar at the bottom part of RC columns after the final loading cycle.

Cyclic response of the RS model (RC frame + steel frame) is depicted in Fig. 8b. The RS specimen exhibited a ductile behavior and the observed cracks on the RC frame were below acceptable limits in width and amount (Maximum crack width: 0.4 mm). The inelastic type of hysteretic behavior seen in Fig. 8b is due to the cracks and plastic behavior of the mortar zone. In fact, distributed cracks were observed in the mortar zone connecting the RC and steel frames (maximum crack width: 1 mm).The steel frame strain measurements indicated that the steel frame remained elastic (as per the design intent) up to the retrofit target drift angle of 1/150. At 2% story drift, significant cracks developed at the mortar connection and tearing of steel frame flange welds was

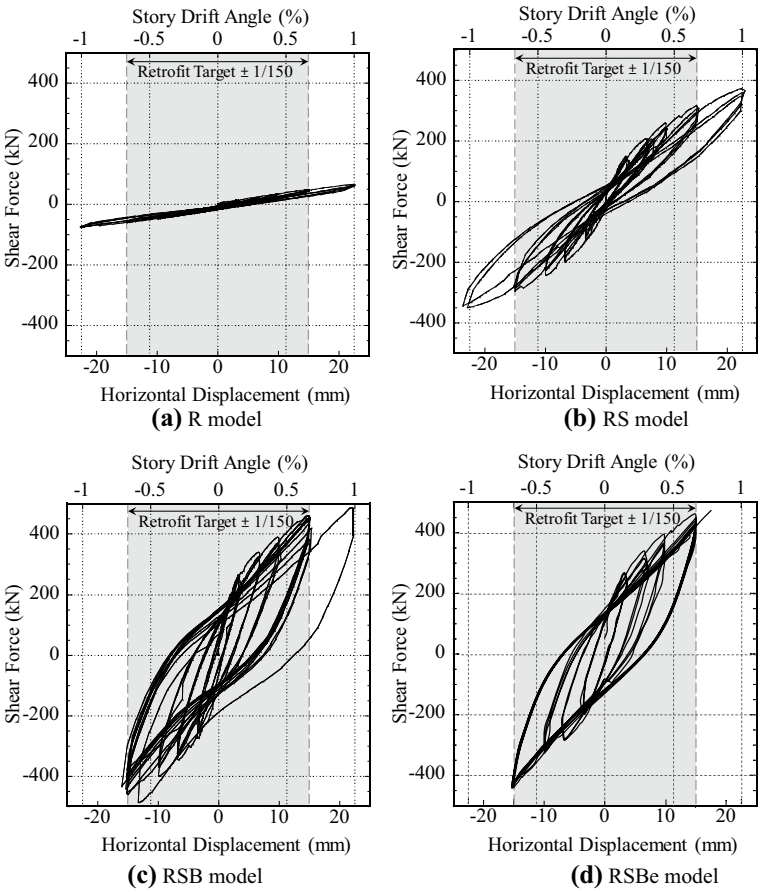

Fig. 8 Load versus drift responses of **a** R, **b** RS, **c** RSB, **d** RSBe

observed near the upper and lower corners. At maximum deformation, concrete spalling and bending failure were observed with exposed rebar at the bottom of the RC columns.

Figure 8c shows the hysteretic response of RSB model (RC frame + steel frame + BRB). The BRB core yielded at around 0.15% story drift and exhibited stable energy dissipation through the retrofit target of 1/150 story drift. Energy dissipation was significantly enhanced relative to the R or RS specimens. Small cracks were observed at the surface of the RC columns near the BRB connection zone at 0.3% drift (maximum width: 0.7 mm) and at the mortar connection at 1/150 drift, similar to the RS specimen (maximum width: 0.9 mm). As the horizontal shear reached 90% of the actuator capacity at 1/150 drift, testing was continued at this level to reach a total of 9 cycles at the target story drift, confirming stable energy dissipation. The actuator capacity was exceeded during the first cycle at 1% drift. Similar to the RS specimen, the strength exceeded the estimated capacity due to strong composite interaction between the RC and steel frames, which is explained in the following section.

Response of the RSBe model (RC + external steel frames + BRB) demonstrated stable energy dissipation up to the retrofit target story drift of 1/150 as shown in Fig. 8d. Small

cracks were primarily observed on the top and bottom of the RC columns (maximum width: 0.5 mm), but no significant cracks were noted. Similar to the RSB specimen, 9 cycles were conducted at 1/150 target drift, confirming stable energy dissipation. The test was terminated during the first cycle at 1% drift as the horizontal force exceeded the actuator capacity.

Figure 8 clearly shows the increase in lateral strength introduced by both the steel frame and BRB (at 1/150, R: 75.2 kN, RS: 315.5 kN, RSB: 459.0 kN and RSBe: 459.2 kN). Furthermore, there is a dramatic increase in hysteretic energy dissipation capacity, primarily attributed to the BRB. It was also observed that the cracks in the mortar zone were less significant in the specimens retrofitted with BRB (RSB and RSBe) than the cracks observed in RS model.

As shown in Fig. 8, the retrofitted system stiffness is significantly higher compared to the bare frame, which will result in a decrease in the fundamental period, and accordingly an increase in the lateral force demand may be expected. However, the fundamental period of the target low-rise school buildings (Fig. 2) investigated in this research are already in the plateau of the design acceleration spectrum of the Turkish code (acceleration constant zone) and an increase in force demand is not expected. In addition, the increased/added damping is obvious to reduce the dynamic response of the structure.

Damage at the base of the North column (left side in Figs. 2, 3, 4) at 1/150 drift is shown in Fig. 9 for the three specimens. While concrete spalling is observed and some concentrated cracks were visible on R specimen, a distributed plastic hinge (or distributed plasticity) is clearly visible for the RS and RSB specimens. In other words, the retrofit schemes have provided a damage controlled behavior. Such smaller cracks can be easily fixed following an earthquake.

Dissipated hysteretic energy in each cycle up to the retrofit target story drift is shown in Fig. 10a. As presented in the figures and as expected, the amount of dissipated hysteretic energy is the largest in retrofit models (RSB and RSBe) when compared to RS and R models at the same drift levels.

Equivalent damping ratio, h_{eq} is also a useful information for evaluating the seismic effectiveness of a retrofit scheme and calculated for each cycle of tests up to the retrofit target story drift level as shown in Fig. 10b. Equivalent damping ratio can be defined with the widely used following equation:

$$h_{eq} = \frac{\Delta W}{4\pi W_e} \tag{1}$$

Here ΔW is the energy dissipated by the hysteretic behavior and calculated from the loop area of each cycle. Also, W_e is the equivalent potential energy of each cycle that basically corresponds to the equivalent stiffness on a certain displacement and it is obtained

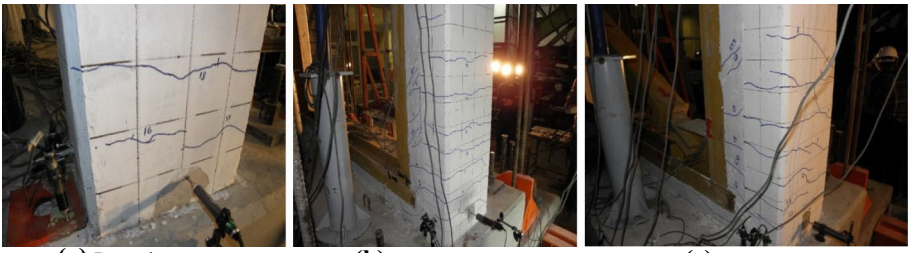

(a) R specimen **(b)** RS specimen **(c)** RSB specimen

Fig. 9 Damage at North column bottom end at retrofit target story drift angle (1/150)

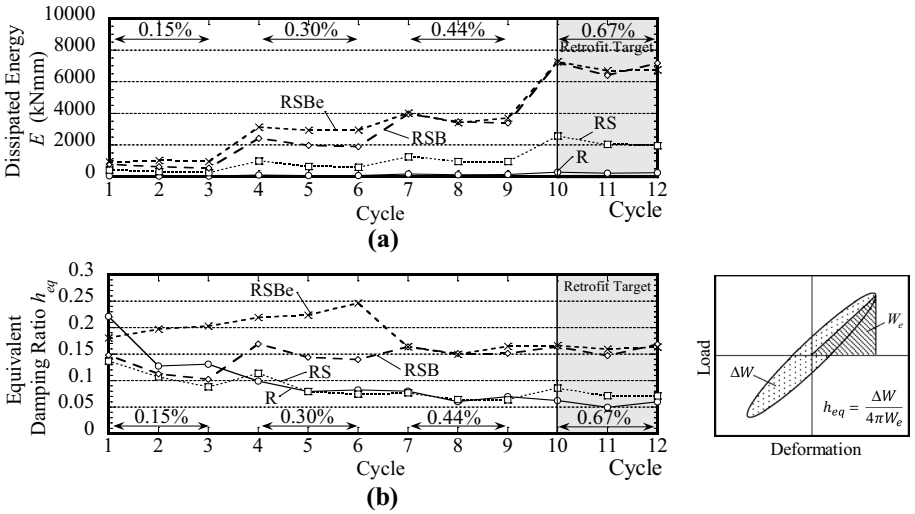

Fig. 10 **a** Dissipated hysteretic energy, **b** equivalent damping ratio in each test cycle until retrofit target story drift angle of 1/150 (0.67%)

at the maximum displacement of that cycle. In this test program, the cyclic loading was quasi-static and due to lack of velocity, structural inherent damping is not observed. Therefore, effect of random cycles and structural viscous damping are neglected. Evaluation of equivalent damping ratio is not stable for relatively small story drift ratios as the hysteretic energy is almost zero during small drifts. However, after 0.30% story drift, h_{eq} is stable. At the target drift ratio, h_{eq} for retrofit models RSB and RSBe is approximately 17% which is almost 3 times those of RS and R models.

4 Estimation of hysteretic behavior and dissipated energy

Total hysteretic behavior can be considered as a summation of the RC frame, steel frame (SF), and BRB contributions, in this section, excluding the composite action. The initial frame stiffness of a single bay RC or steel frame is calculated according to Eq. (2), based on the simplified model shown in Fig. 11. In this equation, E is the Young's modulus for frame material, $I_{c\ left}$, $I_{c\ right}$ and I_b are the uncracked moments of inertia for the left and right columns and

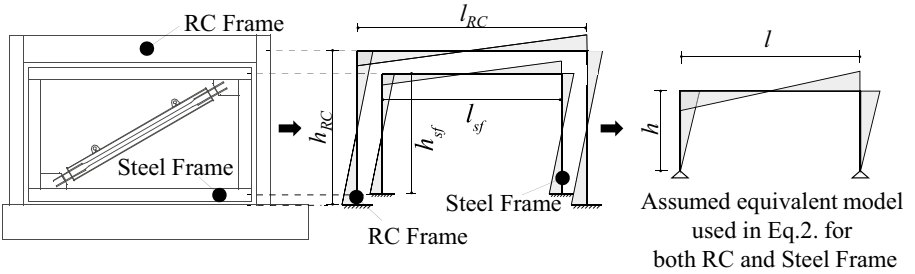

Fig. 11 Stiffness evaluation model

beam, respectively, h is the story height and l is the span of the frame whether it is the RC or steel frame. The story shear stiffness given by Eq. (2) for a single moment frame bay assumes that the moment diagram has a mid-height inflection point, as shown in Fig. 11. This simplifies the frame to a half height pinned-base portal frame.

$$k = 1/\left(\frac{h^3}{12EI_{cleft}} + \frac{h^3}{12EI_{cright}} + \frac{h^2 l}{12EI_b}\right) \tag{2}$$

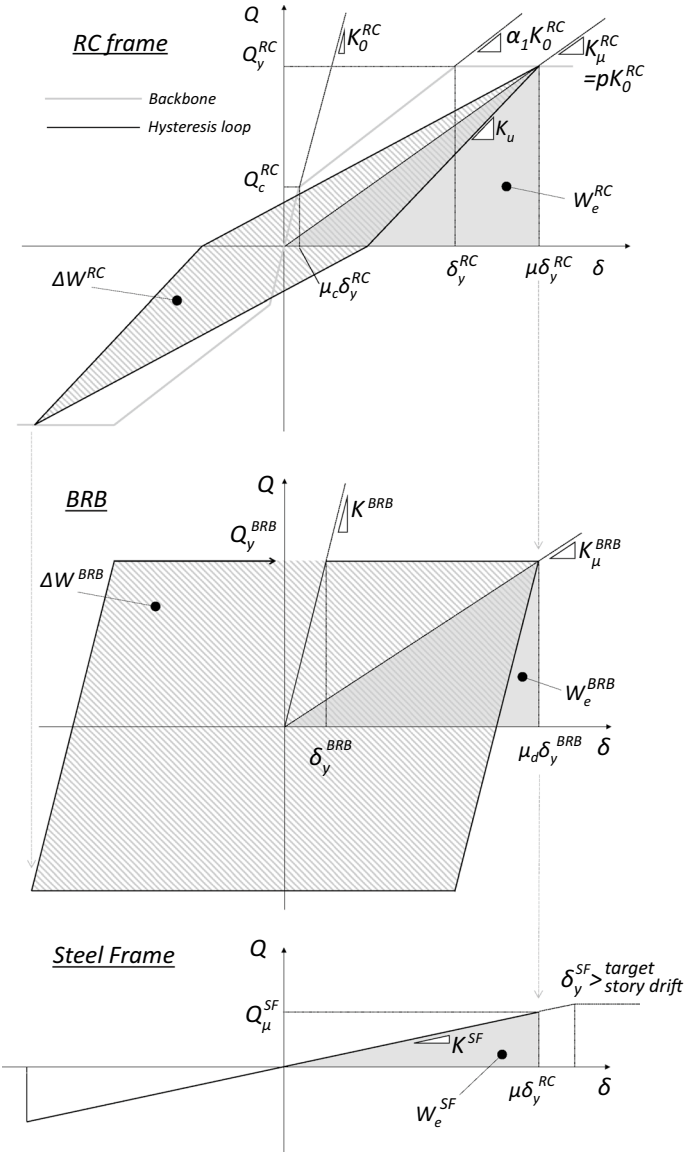

Fig. 12 Hysteresis models of RC frame, steel frame and BRB

Following the equivalent linearization approach, the estimated hysteresis for each component is shown in Fig. 12 and related hysteretic energy (ΔW) equations are given in Eqs. (3) and (4). Equivalent potential energy (W_E) of RC frame and total retrofit structure are expressed in Eqs. (5) and (6), respectively. Dissipated hysteretic energy and equivalent potential energy formulas given in Eqs. (3) through (6) are simply obtained from Fig. 12 and symbols are shown on these figures. Actually, these are the shaded areas under the curves as shown in Fig. 12. The RC frame hysteresis assumes that cracking occurs at a ductility ratio of $\mu_c = 0.1$, a base shear at cracking equal to 1/3 the yield strength $Q_y^{RC}/Q_C^{RC} = 3$, a cracked-to-initial stiffness ratio of $\alpha_1 = 0.22$, yield story drift of 1/225 rad and perfectly plastic post-yield behavior. Takeda's tri-linear degrading model (Takeda et al. 1970) is used for the unloading stiffness K_u, and p is the secant stiffness ratio, which is calculated using Eq. (3) b. The BRB yield force was obtained from the average coupon test yield stress, and the steel frame is assumed and designed to remain elastic in the target retrofit drift range.

Dissipated hysteretic energy:

$$\Delta W^{RC} = \begin{cases} 2K_0^{RC}\left(\mu\delta_y^{RC}\right)^2 \frac{p\mu_c(1-p)}{\mu_c+p\mu} & (\mu_c < \mu \le 1) \\ 2K_0^{RC}\left(\mu\delta_y^{RC}\right)^2 \left[p - \frac{p^2(1+\mu_c)\mu^{\lambda}}{\mu_c+p\mu}\right] & (\mu > 1) \end{cases} \tag{3-a}$$

where

$$p = \begin{cases} \frac{\mu_c+\alpha_1(\mu-\mu_c)}{\mu} & (\mu_c < \mu \le 1) \\ \frac{\mu_c+\alpha_1(1-\mu_c)}{\mu} & (\mu > 1) \end{cases} \tag{3-b}$$

$$\Delta W^{BRB} = 4K^{BRB}\left(\mu_d - 1\right)\left(\delta_y^{BRB}\right)^2 \tag{4}$$

Equivalent potential energy:

$$W_e^{RC} = \frac{1}{2}K_{\mu}^{RC}\left(\mu\delta_y^{RC}\right)^2 \tag{5}$$

$$W_e^{\Sigma} = W_e^{RC} + W_e^{BRB} + W_e^{SF} = \begin{cases} \frac{1}{2}\left(\mu\delta_y^{RC}\right)^2\left(K^{BRB} + K^{SF} + pK_0^{RC}\right); & \mu_c < \mu \le \frac{\delta_y^{BRB}}{\delta_y^{RC}} \\ \frac{1}{2}\left(\mu\delta_y^{RC}\right)^2\left(\frac{K^{BRB}}{\mu_d} + K^{SF} + pK_0^{RC}\right); & \mu > \frac{\delta_y^{BRB}}{\delta_y^{RC}} \end{cases} \tag{6}$$

In Fig. 12 and Eqs. 3 to 6, Q_y^{RC} is the yield shear force, Q_c^{RC} is the cracking shear force, δ_y^{RC} is the yielding displacement, δ_c^{RC} is the cracking displacement, K_0^{RC} is the initial stiffness and K_{μ}^{RC} is the post-yielding secant stiffness of the RC frame ($K_{\mu}^{RC} = pK_0^{RC}$). Also, δ_y^{BRB} is the yielding displacement and μ_d is the ductility ratio of BRB.

Before comparing the hysteretic energy dissipations, the test response of each component was isolated for the three cycles at 0.67% story drift, as shown in Fig. 13. The RC frame (Fig. 13a) force–displacement response has a good agreement with the estimated stiffness and strength, but the experimental loop area is slightly smaller, indicating a less dissipated energy. It should be noted that Fig. 13b is not the pure BRB response, as this figure was obtained by subtracting the RS model test response from the full RSB model

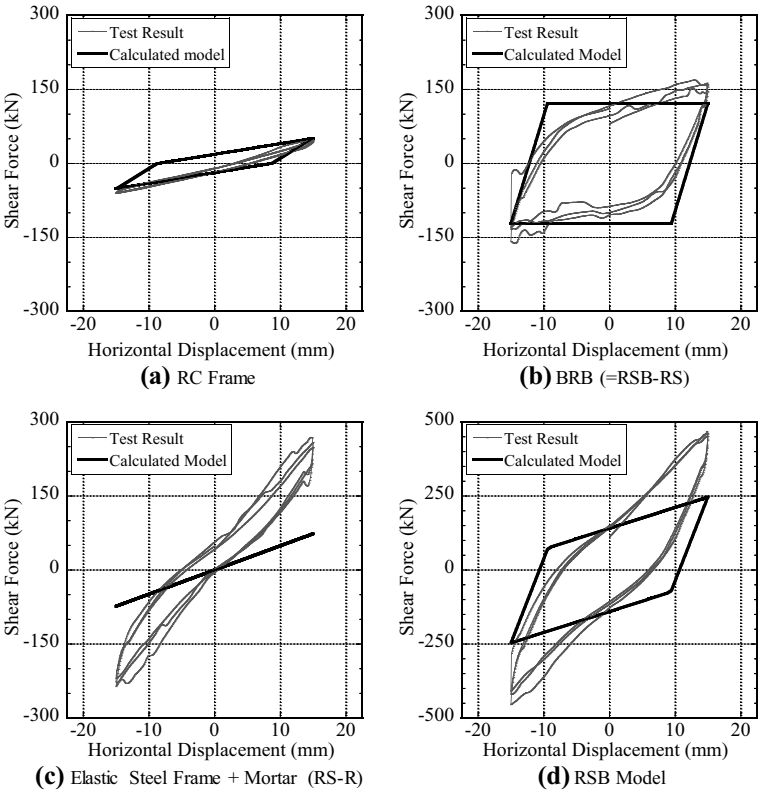

Fig. 13 Load-displacement relationships of each component at 1/150 target story drift cycles

test, which adds both the BRB and effect of gusset plates on the stiffness of the steel frame (RSB model has gussets, whereas RS has no gussets). Therefore, while the yield forces and energy dissipation per loop are in good agreement, the experimental strain hardening appears to be larger than nominal levels and far from an elastic-perfectly plastic idealization. The portion attributed to strain hardening is approximately 1% of the initial stiffness of BRB and hereafter the calculated hysteresis is modified accordingly. From the figure, initial BRB stiffness is calculated to be $K^{BRB} = 44.22$ kN/mm, which is compatible with the initial design that suggested $K^{BRB}/K_0^{RC} = 2.6$ is valid.

Overall response of the combined mortar and steel frame behavior was obtained by deducting the cyclic response of R specimen from the RS specimen and is shown in Fig. 13c. This includes the composite behavior of the total cross-section, as well as energy dissipation due to mortar cracking, yielding of the post-fixed anchors, shear studs and mortar rebar. In this study, energy dissipation within the mortar zone (i.e. the transition zone) or steel frame is conservatively neglected, with these components assumed to remain elastic within the target story drift. However, the composite action between the mortar, steel frame, and RC frame is substantial and is studied in greater detail in the latter sections. Finally, the total retrofitted system response is shown in Fig. 13d.

As previously discussed, equivalent damping ratio is obtained by hysteretic energy and equivalent potential energy of the cyclic behavior (Eq. 1). The calculated and observed

Table 2 Energy dissipations and equivalent damping ratios (at 0.67% story drift)

Cycle		Hysteretic energy (kN mm)			Equivalent potential energy (kN mm)			Equivalent damping ratio		
		Calc.	Test	Test/calc.	Calc.	Test	Test/calc.	Calc.	Test	Test/calc.
RSB model	1	6531	7049	1.08	1855	3514	1.89	0.28	0.16	0.57
	2		6227	0.95		3478	1.87		0.14	0.51
	3		6982	1.07		3401	1.83		0.16	0.58

dissipated energies and corresponding equivalent damping ratios during 3 cycles of the test at the target drift are compared in Table 2. While the hysteretic energy calculation seems accurate compared to the test results, in reality, the corresponding values for RC frame and BRB are slightly overestimated (Fig. 13a, b) and this is balanced by the neglected hysteretic energy of the mortar zone (Fig. 13c). On the other hand, by neglecting composite action, total equivalent stiffness and accordingly the equivalent potential energy are substantially underestimated as seen on the table. As a result, an overestimated equivalent damping ratio is obtained, which is not conservative.

5 Estimation of the composite behavior

As indicated by the tests results, the equivalent stiffness and shear strength of the retrofitted specimens are higher than anticipated due to the strong composite interaction between the steel frame, mortar, and RC frame. To quantify the degree of composite action, the stiffness of the steel frame and mortar obtained from the tests is compared to the estimated steel frame stiffness across a range of story drifts in Fig. 14. The composite action is expected to reduce with increasing displacement levels, due to crack propagation through the mortar. This general trend is observed in Fig. 14, which shows the ratio of the secant stiffness for each cycle during the RSB model test to the calculated steel frame stiffness (denoted as a_c).

As the figure suggests, a_c is quite high in the first cycles, but soon reduces as the number of cycles and drift increases due to loss or weakening of the composite action. At the target 1/150 story drift, a_c is approximately 3.3 for RSB model (for the RSBe model a_c is approximately 2.8). All composite action is eventually lost by the end of the test following the cycles at 1.0% and 2.0% story drift, with a_c finally reducing to 1.0. This is consistent with the observed cracking pattern, as large cracks had begun to form a zigzag pattern at the target drift, tracing the post-fixed anchor and shear studs positions. Due to the complexities

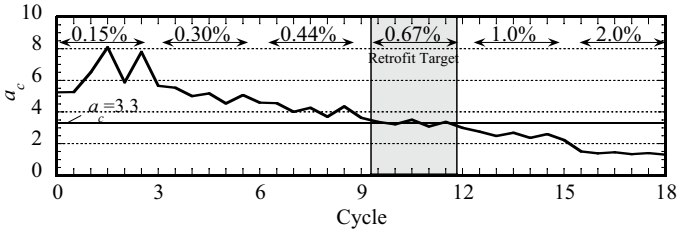

Fig. 14 Test/estimated steel frame stiffness ratio

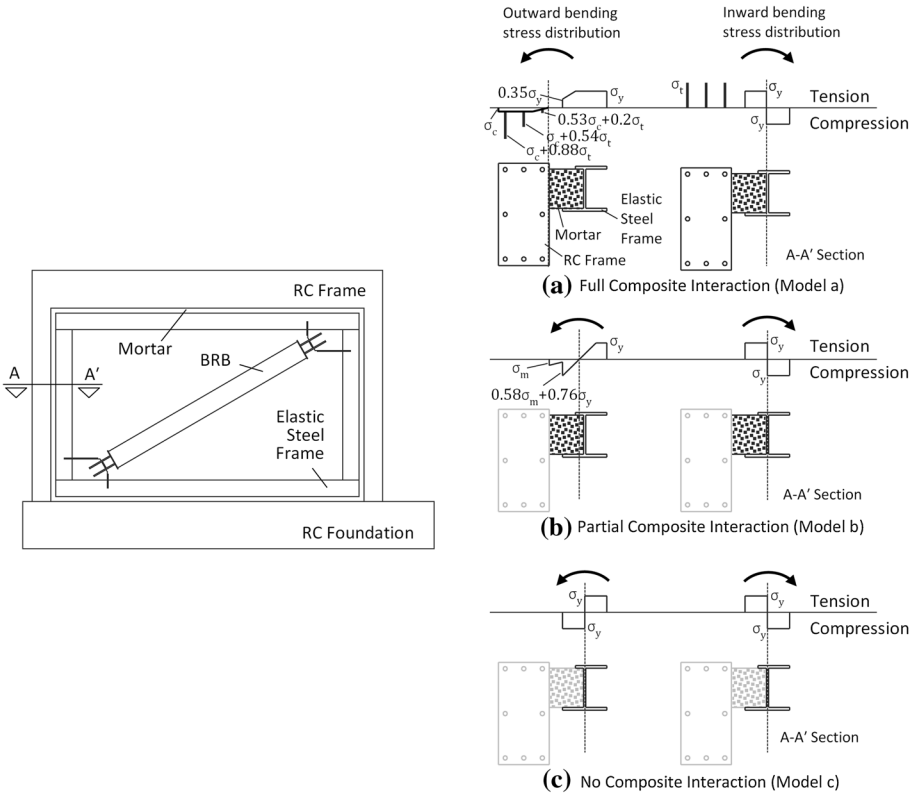

Fig. 15 Assumed composite interaction models for RSB retrofit option

in dynamically updating the composite stiffness, it is desirable to select an effective composite model.

Three different composite sections/levels are considered in Fig. 15 in order to investigate and better explain the observed composite behavior of RSB retrofit option in the tests. Similar section models can be developed for RSBe model where the steel beam application is different (please check Fig. 4). The first (Model-a) represents the full (upper bound) composite behavior where the steel frame, mortar, and RC frame act as a single monolithic section. In Model-b, just the steel frame and mortar act compositely, and in Model-c all three components act independently, corresponding to the initial estimate shown in Fig. 13d and producing the lower bound stiffness. While all three models are applicable at various drift ranges, the partial composite behavior Model-b offers the best compromise between conservatively estimating the story drift and equivalent damping, and best corresponds to the stiffness at the target drift.

To estimate the partial-composite frame stiffness (Model-b), the cross-section properties are first calculated for each component under both inward and outward bending actions. Elastic composite stiffness of the steel frame and mortar zone assembly is then calculated by using Eq. (2), with Young's modulus of the mortar and steel taken to be $E_c = 30{,}766$ N/mm^2 and $E_s = 205{,}000$ N/mm^2, respectively. The revised stiffness estimate has a good agreement with the test results for the steel frame mortar assembly at the target story drift

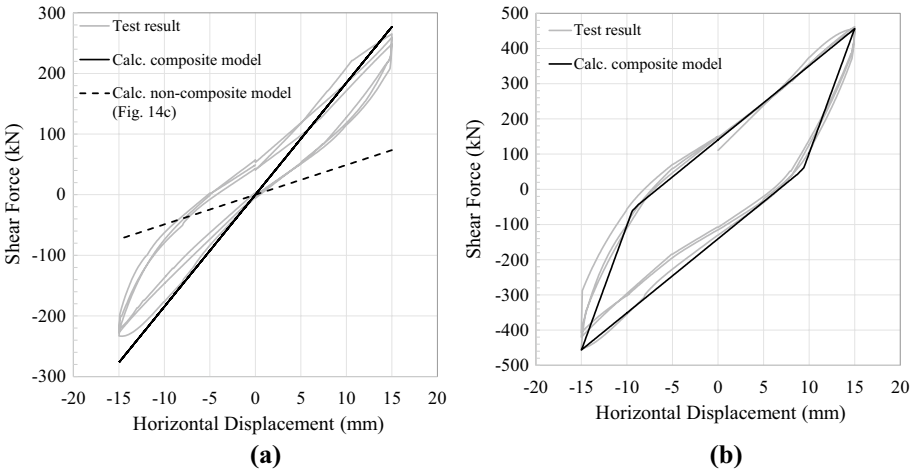

Fig. 16 Test versus estimated behavior at 1/150 target story drift: **a** steel frame + mortar, **b** RSB model

(Fig. 16a). It should be noted that the effect of gussets is included in the calculated stiffness by adjusting the frame spans in Eq. (2), assuming that the frame is infinitely rigid along the gusset length. Strain hardening of the BRB is assumed to be approximately 1% of the initial stiffness and included in the total behavior. After including the composite effect contribution, the total calculated behavior of the retrofit model shows a good correspondence with test result as shown in Fig. 16b.

The equivalent potential energy and damping ratio at the target retrofit displacement are highly sensitive to the shear stiffness and strength of the structure. The equivalent potential energy given by Eq. (6) for $\mu > \delta_y^{BRB}/\delta_y^{RC}$ is modified in Eq. (7) to include the enhanced steel frame stiffness a_c and BRB strain hardening ratio β.

$$W_e^{\Sigma} = W_e^{RC} + W_e^{BRB} + W_e^{SF} = \frac{1}{2}K_0^{RC}\left(\mu\delta_y^{RC}\right)^2\left(\frac{(\mu_d - 1)\beta + 1}{\mu_d}K^{BRB} + a_c K^{SF} + pK_0^{RC}\right) \tag{7}$$

Table 3 Energy dissipation and equivalent damping ratio with proposed composite model

Cycle		Hysteretic energy (kN mm)			Equivalent potential energy (kN mm)			Equivalent damping ratio		
		Calc.	Test	Test/calc.	Calc.	Test	Test/calc.	Calc.	Test	Test/calc.
RSB	1	6531	7049	1.08	3327	3511	1.06	0.16	0.16	1.02
	2		6227	0.95		3459	1.04		0.14	0.92
	3		6982	1.07		3388	1.02		0.16	1.05
RSBe	1	6471	7254	1.12	3653	3473	0.95	0.14	0.17	1.18
	2		6694	1.03		3338	0.91		0.16	1.13
	3		6754	1.04		3288	0.90		0.16	1.17

The equivalent damping ratio with its components is once again calculated and compared with the test result, taking the proposed composite behavior into account, this time both for RSB and RSBe specimens. The comparison is shown in Table 3 for the cycles at the 0.67% retrofit target drift. In that table, the equivalent damping ratio is calculated by using Eq. (1) based on the equivalent potential energy obtained by Eq. (7), adopting a_c to be 3.3 (RSB) and 2.8 (RSBe). After implementing the proposed composite behavior model in the equations, the accuracy of the equivalent damping ratio calculation greatly improves and a very good agreement is obtained with the actual test results.

Similar calculations were performed for the loading cycles at 0.3% and 0.44% story drifts. The average over 3 cycles at each loading amplitude was considered when determining a_c. Good agreement is achieved between the test results and calculated model, as shown in Fig. 17.

6 Conclusions

Near full-scale cyclic tests were conducted on a retrofitted single bay RC frame with BRBs installed within supplementary steel frames, which were designed to remain elastic. Multiple specimens were tested to study each component of the proposed retrofit scheme, providing an insight into the behavior and contribution of the existing RC frame, new steel frame, mortar connection, and BRB. Particular emphasis is paid on the composite behavior between the RC and steel frame, as the mortar connection is expected to be nonlinear and is a key component of the retrofitted frame. The specimens were tested under a gradually increasing, displacement based cyclic loading protocol developed specifically for this test program. The following conclusions can be drawn from this near full-scale experimental work:

1. The addition of the BRB and steel frame improved the structural performance significantly. At the 1/150 retrofit target story drift, no significant structural damage was

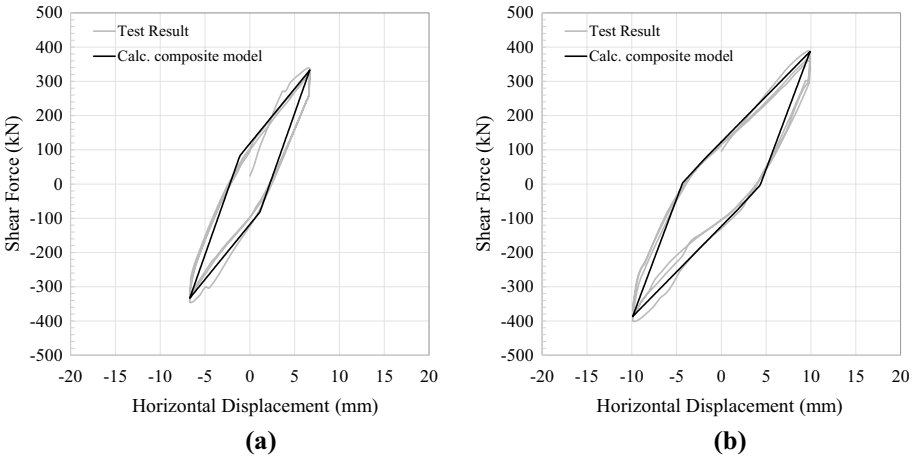

Fig. 17 Test results versus calculated models for RSB model: **a** 0.30% story drift and $a_c = 5.0$, **b** 0.44% story drift and $a_c = 4.1$

observed in the retrofitted specimen. The lateral strength increased by a factor of 9 compared to the bare RC frame and the energy dissipation by a factor of 3. No global or local buckling of the BRB was observed.

2. Up to the retrofit target story drift, the steel frame strain measurements were generally at or below the yield level, indicating that the steel frame can remain elastic up to a target retrofit level. This significantly enhances the self-centering properties of the retrofitted frame during a major earthquake. In actual applications, as the BRBs possess fuller and stable hysteretic behavior under substantially large deformations, the SF can also be designed to remain elastic in a wider drift range considering larger seismic demands or larger target drifts. Strain gauges were also attached to the rebar in the RC frame. Although several indicated yielding, structural integrity of the RC frame was maintained, with minimal cracking and ductile behavior observed with controlled distributed plasticity along the RC members.
3. Composite behavior between the RC and steel frame was extensively investigated for the first time in this work and a partial-composite model is proposed where composite action is only considered between the steel frame and mortar. The proposed model accurately estimates the overall cyclic behavior, enabling accurate assessment of the dissipated energy during preliminary design stages.

In summary, the proposed seismic retrofit scheme with two application options, consisting of a BRB installed with an elastically designed steel frame, is an effective solution for sub-standard RC buildings. In this research, the authors have focused on the composite behavior of retrofit system, which is crucial in seismic design of such systems. Although the results cannot be directly used for any random building, they sufficiently explain how the composite behavior could be estimated. Further research is underway to study the effect of various configurations over multiple stories and other types of energy dissipating devices.

Acknowledgements Buckling-restrained braces used in the tests were kindly provided by Nippon Steel. Emek Prefabrik, Hilti, and BASF are acknowledged for their invaluable support for building the test specimens. All tests are carried out in the Earthquake and Structural Engineering Laboratory (STEEL) of Istanbul Technical University (ITU) where the assistance of staff and graduate students is greatly appreciated. Conclusions, and recommendations expressed in this paper are those of the authors and do not necessarily reflect those of the sponsors.

References

Barbagallo F, Bosco M, Marino M, Rossi PP (2019) Seismic design and performance of dual structures with brbs and semi-rigid connections. J Constr Steel Res 158:306–316. https://doi.org/10.1016/j.jcsr.2019.03.030

Celik OC, Bruneau M (2009) Seismic behavior of bidirectional-resistant ductile end diaphragms with buckling restrained braces in straight steel bridges. Eng Struct 31(2):380–393

Celik O, Berman J, Bruneau M (2005) Cyclic testing of braces laterally restrained by steel studs. ASCE J Struct Eng 131(7):1114–1124

Chou C-C, Liu J-H (2012) Frame and brace action forces on steel corner gusset plate connections in buckling-restrained braced frames. Earthq Spectra 28(2):531–551

Corte GD, D'Aniello M, Landolfo R (2015) Field testing of all-steel buckling-restrained braces applied to a damaged reinforced concrete building. J Struct Eng 141:0733–9445

Di Sarno L, Manfredi G (2012) Experimental tests on full-scale RC unretrofitted frame and retrofitted with buckling-restrained braces. Earthq Eng Struct Dyn 41(2):315–333

Dinu F, Bordea S, Dubina D (2012) Strengthening of non-seismic reinforced concrete frames of buckling restrained steel braces. In: Proceedings of the conference on behavior of steel structures in seismic areas (STESSA 2012), Santiago de Chile

El-Bahey S, Bruneau M (2011) Buckling restrained braces as structural fuses for the seismic retrofit of reinforced concrete bridge bents. Eng Struct 33:1052–1061

Freddi F, Tubaldi E, Ragni L, Dall''sta A (2012) Probabilistic performance assessment of low-ductility reinforced concrete frames retrofitted with dissipative braces. Earthq Eng Struct Dyn 42(7):993–1011. https://doi.org/10.1002/eqe.2255

Fujimoto M, Wada A, Saeki E, Takeuchi T, Watanabe A (1990) Development of unbonded brace. Q Column 115:91–96

Fujishita K, Bal A, Sutcu F, Celik OC, Takeuchi T, Matsui R, Terashima M (2015) Comparing hysteretic behavior of buckling restrained braces (BRBs) with bolted and welded end connections. In: 8t^{h} international symposium on steel structures, November 5–7, 2015, Jeju, Korea

Japan Building Disaster Prevention Association (JBDPA) Standard for Seismic Diagnosis of Existing Reinforced Concrete Structures—English Version (2001)

Kiggins S, Uang C-M (2006) Reducing residual drift of buckling-restrained braced frames as a dual system. Eng Struct 28(11):1525–1532. https://doi.org/10.1016/j.engstruct.2005.10.023

Mahrenholtz C, Lin PC, Wu AC, Tsai KC, Hwang SJ, Lin RY, Bhayusukma MY (2015) Retrofit of reinforced concrete frames with buckling-restrained braces. Earthq Eng Struct Dyn 44:59–78

Palazzo G, López-Almansa F, Cahís X, Crisafulli F (2009) A low-tech dissipative buckling restrained brace: design, analysis, production and testing. Eng Struct 31:2152–2161

Pan KY, Wu AC, Tsai KC, Li CH, Khoo HH (2016) Seismic retrofit of reinforced concrete frames using buckling-restrained braces with bearing block load transfer mechanism. Earthq Eng Struct Dyn 45(14):2303–2326

Qu Z, Maida Y, Sakata H, Wada A, Kishiki S, Maegawa T et al (2012) Numerical assessment of seismic performance of continuously buckling restrained braced RC frames. In: Proceedings of the 15t^{h} world conference on earthquake engineering (15WCEE), paper #0355, Lisbon

Ozcelik R, Erdil EE (2019) Pseudodynamic test of a deficient RC frame strengthened with buckling restrained braces. Earthq Spectra 35(3):1163–1187

Sabellia R, Mahinb SA, Chang C (2003) Seismic demands on steel braced frame buildings with buckling-restrained braces. Eng Struct 25(5):655–666. https://doi.org/10.1016/S0141-0296(02)00175-X

Sugano S (1989) Study of the seismic behavior of retrofitted reinforced concrete buildings. In: Proceedings of the ASCE'89 structural congress, San Francisco

Sutcu F, Takeuchi T, Matsui R (2014) Seismic retrofitting design method of existing RC buildings with buckling restrained braces. J Constr Steel Res 101:304–313

Takeda T, Sozen MA, Nielsen NN (1970) Reinforced concrete response to simulated earthquakes. J Struct Div ASCE 96(12):2557–2573

Takeuchi T, Wada A (2017) Buckling-restrained braces and applications. JSSI Tokyo Japan

Takeuchi T, Yasuda K, Iwata M (2006) Studies on integrated building façade engineering with high-performance structural elements. In: IABSE conference 2006 (Budapest), pp 442–443

Takeuchi T, Ozaki H, Matsui R, Sutcu F (2014) Out-of-plane stability of buckling-restrained braces including moment transfer capacity. Earthq Eng Struct Dyn 43(6):851–869

Takeuchi T, Matsui R, Saki M (2016) Out-of-plane stability assessment of buckling-restrained braces including connections with chevron configuration. Earthq Eng Struct Dyn 45(12):1895–1917

Tsai K-C, Hsiao P-C, Wang K-J, Weng Y-T, Lin M-L, Lin K-C, Chen C-H, Lai J-W, Lin S-L (2008) Pseudo-dynamic tests of a full-scale CFT/BRB frame—part I: specimen design. Exp Anal Earthq Eng Struct Dyn 37:1081–1098. https://doi.org/10.1002/eqe.804

TS500-Requirements for Design and Construction of Reinforced Concrete Structures (1975, 1984) Turkish Standards Institute, Ankara, Turkey

Turkish Disaster and Emergency Management Presidency, Turkish Building Seismic Code (TBSC-2018) (2018) (in Turkish)

Turkish Ministry of Public Works and Housing, Specification for Structures to be Built in Disaster Areas (SSBDA) (1975) (in Turkish)

Wakabayashi M, Nakamura T, Kashibara A, Morizono T, Yokoyama H (1973) Experimental study of elasto-plastic properties of precast concrete wall panels with built-in insulating braces. In: Proceedings of the annual convention of the architectural Institute of Japan, pp 1041–1044 **(in Japanese)**

Watanabe A, Hitomi Y, Saeki E, Wada A, Fujimoto M (1988) Properties of brace encased in buckling-restraining concrete and steel tube. In: Proceedings of the 9t^{h} world conference on earthquake engineering, Tokyo-Kyoto

Wu A-C, Lin P-C, Tsai K-C (2013) High-mode buckling responses of buckling-restrained brace core plates. Earthq Eng Struct Dyn 43(3):375–393

Yooprasertchai E, Warnitchai P (2008) Seismic retrofitting of low-rise non-ductile reinforced concrete buildings by buckling-restrained braces. In: Proceedings of 14t^{h} world conference on earthquake engineering (14WCEE), Beijing